Fluid Phase Equilibria 522 (2020) 112741

Contents lists available at ScienceDirect

Fluid Phase Equilibria

journal homepage: www.elsevier.com/locate/fluid

Ice formation and growth in supercooled water–alcohol mixtures: Theory and experiments with dual fiber sensors

Markus Solberg Wahl [a], Ailo Aasen [b, c], Dag Roar Hjelme [a], Øivind Wilhelmsen [b, c, *]

[a] Norwegian University of Science and Technology (NTNU), Department of Electronic Systems, 7491, Trondheim, Norway
[b] Norwegian University of Science and Technology (NTNU), Department of Energy and Process Engineering, 7491, Trondheim, Norway
[c] SINTEF Energy Research, 7034, Trondheim, Norway

ARTICLE INFO

Article history:
Received 23 December 2019
Received in revised form
5 May 2020
Accepted 25 June 2020
Available online 12 July 2020

Keywords:
Heterogeneous nucleation
Phase transitions
Multimode interference
Fiber-optic sensors

ABSTRACT

Increased knowledge on fluid-solid phase transitions is needed, both when they are undesired and can impair process operations, and when strict control is required in fields such as food technology, the pharmaceutical industry and cryogenic CO_2 capture. We present experimental results and theoretical predictions for the solid-formation and melting temperatures of ice in four binary water–alcohol mixtures containing methanol, ethanol, 1-propanol and 1-butanol. A dual fiber sensor set-up with a fiber Bragg grating sensor and a thin-core interferometer is used to detect the solid-formation. The predictions of melting temperatures with the cubic plus association equation of state combined with an ice model are in good agreement with experiments, but deviations are observed at higher alcohol concentrations. The measured degree of supercooling displays a highly non-linear dependence on the alcohol concentration. A heterogeneous nucleation model is developed to predict the solid-formation temperatures of the binary alcohol–water mixtures. The predictions from this model are in reasonable agreement with the measurements, but follow a qualitatively different trend that results in systematic deviations. In particular, the predicted degree of supercooling is found to be an essentially colligative property that increases smoothly with alcohol concentration. Experimental results are also presented for the growth rate of ice crystals in water–ethanol mixtures. For pure water, the measured crystal growth rate is 10.2 cm/s at 16 K supercooling. This is in excellent agreement with previous results from the literature. The crystal growth rate observed in ethanol–water mixtures however, can be orders of magnitude lower, where a mixture with 2% mole fraction ethanol has a growth rate of 2 mm/s. Further work is required to explain the large reduction in crystal growth rate with increasing alcohol concentration and to reproduce the behavior of the solid-formation temperatures with heterogeneous nucleation theory.

1. Introduction

It is important to predict and control the formation of a solid-phase in numerous industries. Precipitation of inorganic salts from aqueous solutions can impair operation of heat exchangers and production of oil and natural gas, which causes significant economical losses in the industry [1,2]. Aggregate-state control is also important in novel process configurations for liquefaction of hydrogen that involve helium–neon mixtures [3]. Precipitation of solid CO_2 from natural gas mixtures must be controlled to avoid constricting or plugging pipelines, which can cause a sudden and dangerous increase in pressure [4,5]. Although CO_2-frosting is mostly seen as a detrimental effect, it can also be used to separate the unwanted gas from the natural gas mixture [6]. Increased knowledge about phase transitions is important both when they are undesired, and when strict control is needed e.g. in fields such as energy storage systems based on latent heat [7], in food technology [8], to select the desired crystal polymorph in the pharmaceutical industry [9–11], and in biology and intercellular freezing [12–14].

Nucleation refers to the first step in most phase transitions and the formation of an incipient portion of the new phase [15]. In solid-formation, a critical cluster forms by means of thermal fluctuations, either in the bulk of the fluid (homogeneous nucleation), or aided by external surfaces (heterogeneous nucleation). Many experimental and modelling studies have been committed to explore and understand the mechanisms of nucleation [16–20].

* Corresponding author. Norwegian University of Science and Technology (NTNU), Department of Energy and Process Engineering, 7491, Trondheim, Norway.
E-mail address: oivind.wilhelmsen@ntnu.no (Wilhelmsen).

https://doi.org/10.1016/j.fluid.2020.112741

In pure water, homogeneous nucleation of solid crystals has been observed down to − 40°C [18]. In most practical situations however, the nucleation is heterogeneous. This means that impurities in the liquid or surfaces in contact with the fluid promote nucleation by lowering the activation barrier [21]. The molecular dynamic simulations by Sanz et al. showed that nucleation in pure water occurring less than 20 K below the melting point must be heterogeneous [22]. Which materials that promote or inhibit nucleation has been widely studied, but not yet fully understood [19,21,23–28]. Fitzner et al. found that both surface morphology and hydrophobicity are important factors [19].

Due to the activation barrier required to make the first critical cluster, the solid-formation temperature is always below the tabulated melting temperature. For accurate control of precipitation in fluid mixtures, it is of interest to predict and understand at precisely which temperature the solid forms. In this work, we will study the solid-formation temperature and the degree of supercooling that can be achieved in binary water–alcohol mixtures, by use of experiments and theory. Short-chained alcohols have been chosen as examples because they are miscible in both polar and non-polar substances, which makes them versatile solvents [29].

In Ref. [30], the limit of superheating of liquids prior to formation of vapor was predicted to a high accuracy with homogeneous nucleation theory, both for single-component fluids and mixtures. This motivates a hypothesis to be explored in the present work, namely that the solid-formation temperature and the degree of supercooling in mixtures can be predicted by use of heterogeneous nucleation theory for solids. The supercooling is here defined as the difference between the melting temperature and the measured solid-formation temperature.

The theoretical predictions of the liquid-solid phase transition will be compared to experiments. Phase transitions have traditionally been studied through differential scanning calorimetry [31,32] and differential thermal analysis [14,33]. These techniques offer invaluable information on the thermophysical properties of phase transitions, but are traditionally not suited for accurate detection of solid-formation because of their slow response. The increase in temperature due to the release of latent heat can be measured with electronic temperature sensors (e.g. thermocouples, Pt100) [5]. However, because these sensors may act as heat sinks/sources, the accuracy is impaired [34]. Phase transitions can also be observed visually in transparent materials [14,20,35,36]. This is arguably the most accurate of the methods discussed so far. However, transparent containers or windows are necessary, which may not always be experimentally feasible.

Apart from visual methods to detect the onset of phase transitions, most methods are designed to monitor and analyse how the transition progresses. With fiber-optic sensor probes, the solid-formation can be detected directly, either through a change in refractive index or through an associated increase in temperature. Due to their small size and thermal mass, the influence on the measurement is low. Fiber-optic sensors are also chemically inert and mechanically robust, even at cryogenic temperatures [37]. This has in recent years triggered studies into using fiber-optic sensors to detect and study phase transitions [38–42]. Han et al. utilized the special properties of n-octadecane, which has refractive indices above and below that of the fiber in the solid and liquid phase, respectively. This enabled discrimination between the phases based on a guiding or no-guiding condition, which was demonstrated both with a multi-mode fiber interferometer [42] and a Fresnel reflection probe [40]. Mani et al. also used a Fresnel reflection probe to detect solid-formation in aqueous NaCl-solutions. Since only the fiber end-face is in contact with the sample, these point measurements are mechanically very robust, but at the same time sensitive to impurities or bubbles present. Boerkamp et al. measured the rate of crystal growth in $CaCO_3$ scale formation with exposed-core fibers, where the increased scale thickness gradually attenuated the transmitted light [2,38].

In this work, we will use a set-up with a boroscope and two fiber-optic sensors to detect both the solid-formation temperature and the growth rate of the resulting crystal. Details on the experimental set-up and methodology are given in Sec. 2. Next, the theory to predict the melting and solid-formation temperatures of mixtures is presented in Sec. 3. Theoretical predictions are compared to experiments in Sec. 4 before concluding remarks are provided in Sec. 5.

2. Experimental

A schematic of the experimental setup used in this work is shown in Fig. 1. A temperature bath with silicon oil (Hart Scientific, 7103 Micro-bath) and an accuracy of 0.25 K was used to control the temperature. The temperature bath is limited to temperatures above −30°C, which puts a constraint on the range where solid-formation events have been studied. A calibrated temperature sensor (Pt100, 3-wire) with a stainless steel sheath was placed in the bath fluid for confirmation purposes. The test tube containing the sample was placed at the center of the bath, with the sample 10 cm below the silicon oil surface. The open end of the test tube was covered with aluminum foil to reduce losses of heat and mass to the ambient while maintaining atmospheric pressure. Two different test tubes were used, one of glass (Borosil, 27 mL) and one of polypropylene (VWR, 14 mL). The two fiber-optic sensors were secured at positions 1 mm apart, near the center of the sample liquid (see Fig. 1). For visual inspection, a digital boroscope was used to capture images and video. For some of the experiments, the frames of the videos were analysed to measure the size of the growing crystal as a function of time. Further details on this procedure have been included in the supplementary information (SI).

2.1. Fiber-optic detection

The fiber-optic sensor setup is shown in Fig. 1 (right). It consists of a fiber Bragg grating (FBG) sensor, which is sensitive to temperature (T) and strain (ε), and a thin-core (TC) fiber interferometer that is also sensitive to the refractive index (RI) of the surrounding medium (sample). The light source is a broadband laser (FYLA, SCT500), and a grating-based spectrometer (Ibsen, I-MON 512) has been used to capture the combined spectrum from the two sensors. These components are connected through a 2 × 2 50:50 single-mode coupler (Thorlabs, TW1550R5A2). The FBG signal is also attenuated with a variable fiber-optic attenuator to achieve comparable intensitites from the two sensors.

FBG sensors reflect light at the wavelength given by [43].

$$\lambda_B = 2n_{eff}\Lambda, \tag{1}$$

where n_{eff} is the effective RI of the grating and Λ is the grating period. The sensor used (Optromix) is inscribed in an SM1500 fiber, and the reflected wavelength has a full-width half-maximum of 0.2 nm and a reflectivity of 79%. The wavelength shifts as a function of temperature due to thermal expansion and the thermo-optic effect, where the latter accounts for ∼ 95% of the sensitivity [43]. This can be expressed as [44].

$$\Delta\lambda_B = \lambda_B(\alpha + \xi)\Delta T, \tag{2}$$

where α is the thermal expansion coefficient, and ξ is the thermo-optic coefficient.

The TC interferometer is fabricated by splicing a 14.2 mm section of a TC fiber (SM400) fiber to the end of a single-mode fiber

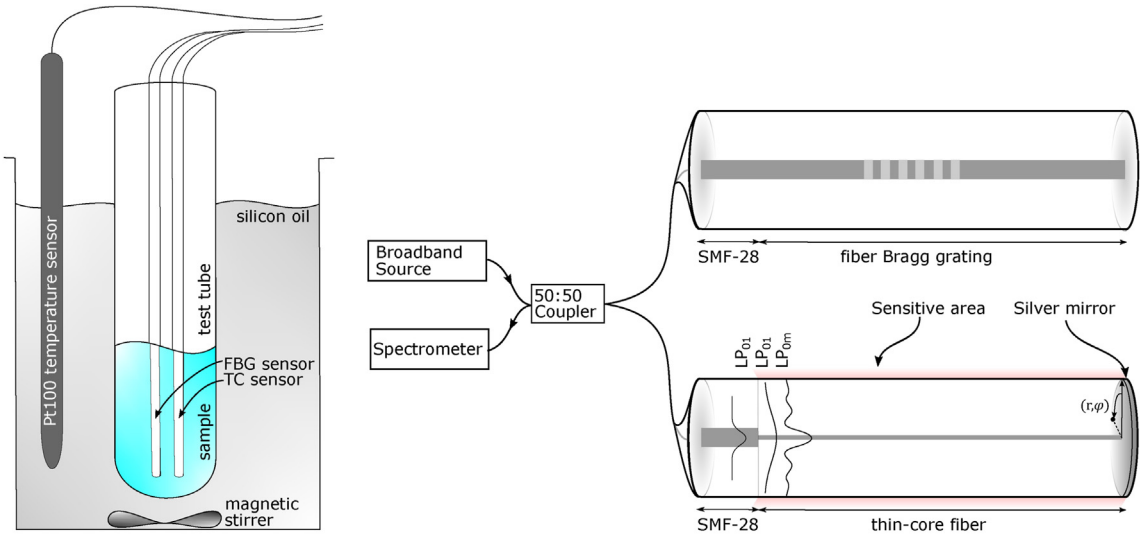

(a) Measurement rig. (b) Fiber-optic sensor configuration.

Fig. 1. A schematic of the experimental set-up (a), which consists of a temperature bath with silicon oil as cooling medium. An electrical Pt100 temperature sensor is used for confirmation. The two sensors are secured at the centre of the test tube that holds the sample. The fiber-optic configuration (b) consists of a broadband source and a spectrometer, which are connected to the two sensors with a 50:50 fiber-optic coupler. The lines connecting the components are all single-mode fibers (SMF-28).

(SMF-28). A silver mirror was deposited at the fiber end-face with the mirror reaction [45], to increase the reflected signal. The mismatch between the cores of the two fibers enables the excitation of an ensemble of cladding modes [46] in the TC fiber, which create an interference spectrum when they are reflected back to the spectrometer. The interference spectrum exhibits characteristic intensity minima, where the modes interfere destructively. This can be expressed as

$$\lambda_{dip,i} = \frac{4L\left[n_{eff}(\lambda, n_{ext}) - n'_{eff}(\lambda, n_{ext})\right]}{2i-1}, \quad (3)$$

where L is the length of the interferometer, n_{eff} and n'_{eff} is the effective index of two modes at wavelength λ and external (sample) RI (n_{ext}). Because the modes are bound by the outer diameter of the fiber, the evanescent field causes the effective indices to be functions of the surrounding RI, as well as the temperature of the sensor.

The dual-sensor configuration enables an independent temperature measurement and a characterization of both the liquid and solid phases. In phase transitions with a low associated latent heat, the TC sensor also enables detection based on changes in the RI.

2.2. Data acquisition and analysis

To control the temperature setpoints and scan rate, an in-house LabVIEW program was developed, which acquires data from the temperature sensors and the spectrometer. The combined spectrum from the two sensors was stored together with the temperature reading every 30 s during cooling. Around the expected solid formation temperature, the acquisition rate was increased to every 10 s.

A typical output spectrum from an experiment is shown in Fig. 2. Here, the FBG peak and the three main TC dips are marked with circles. Only the FBG peak and the first dip of the TC fiber were used for further analysis. Post-processing was performed to determine the exact wavelengths of these features. The FBG peak was fitted to a Gaussian function, whereas the first TC dip was fitted to a polynomial. By tracking these wavelengths as a function of time and temperature, the event of solid formation can be identified.

2.3. Sample preparation

To prepare the samples, deionized (DI) water (< 1.5 μS/cm) was mixed with methanol/ethanol/1-propanol/1-butanol by weight. Concentrations from 0% to 30% (weight) were prepared in intervals of 5%. Because of the limited solubility of butanol in water, only concentrations of 2.5%, 5% and 7.5% were used for the butanol–water mixture. The maximum error estimated for the prepared concentrations was 0.4%, based on the uncertainty disclosed by the manufacturer. The concentrations will be referenced according to their corresponding mol% in the discussion, as colligative effects of the solute are expected to be important.

After preparing the mixtures, the solutions were heated to 50 °C

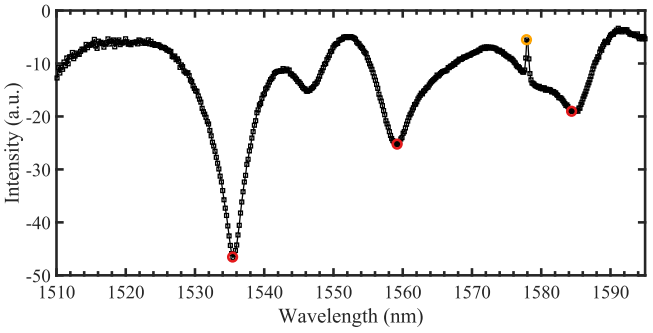

Fig. 2. A typical output spectrum, showing the sum of the reflected intensities from the two sensors as a function of wavelength. Three interference minima (dips) are identified, but only the first is used in interpreting the response. The peak from the FBG sensor has been attenuated as to not saturate the spectrometer, while ensuring acceptable visibility of the interference spectrum. The features of both sensors shift to longer wavelength (red-shift) with increasing temperature. The TC sensor red-shifts for increasing external refractive index.

for 5 hours and stored at room temperature for one week to let them equilibrate [47]. The test tube and fiber-optic sensors were rinsed with acetone, 96% ethanol and DI water before each measurement to remove any contaminants. For the polypropylene test tube, the rinsing procedure influenced the results; this will be further discussed in Sec. 4. The test tube was filled with 6 mL from the sample solution and stabilized at 30 °C for 15 min. Next, the fiber-optic sensors were inserted prior to lowering the temperature down to − 30°C at 0.2 °C/min.

3. Theory

For the mixtures and conditions considered in the present work, the solid-phase crystallizes as pure H_2O [31] with a hexagonal crystal structure known as ice I_h [31,32,48]. The first crystal forms after a certain degree of supercooling by heterogeneous nucleation on the container walls or on the two sensors. A hypothesis that will be explored in this work is that the solid-formation temperature can be determined by heterogeneous nucleation theory. Upon heating, the crystal starts to dissolve at the melting point, i.e. there is no superheating of the crystal. The melting point represents an equilibrium configuration between the fluid and the solid. In the following, we shall elaborate how to determine both the melting temperature (Sec. 3.2) and the solid-formation temperature (Sec. 3.3) by combining theoretical predictions with an equation of state (Sec. 3.1).

3.1. Equations of state for the liquid and the ice

The cubic plus association (CPA) equation of state (EoS) [49] was used to model the liquid phase, with published pure-component parameters from Queimada et al. [50] for water and Oliveira et al. [51] for alcohols. The CPA EoS requires a binary interaction parameter, k_{ij}, to be fitted by use of thermodynamic properties of the binary system considered. This parameter was set to $k_{ij} = -0.1$ for methanol−water and propanol−water, and to $k_{ij} = -0.115$ for ethanol−water and butanol−water; these parameters were validated against experimental vapor−liquid equilibrium composition and density data [52−55]. The CPA equation of state with these parameters has been thoroughly validated in vapor−liquid nucleation studies of water and alcohols [56,57]. Further details and comparisons to experimental data can be found in the SI.

The Gibbs energy of ice I_h was modeled using the equation of state by Feistel and Wagner [58]. The EoS has two adjustable parameters, g_{00} and s_0, corresponding to the reference state for used for Gibbs energy and entropy at 0 K and 1 atm [58]. These parameters were determined from two conditions: (1) reproducing the experimental triple point temperature and pressure (273.16 K and 611.66 Pa) with the combined CPA + Ice model; (2) the enthalpy of fusion at the triple point calculated from the CPA + Ice model equals the experimental value (6007 J/mol). The resulting values were $g_{00} = -2582.47$ kJ/kg and $s_0 = -1483.02$ J/(kg K).

3.2. The melting point

The melting temperature T_{melt} of the mixture was determined by solving for the temperature T that yields equal chemical potential of water in the liquid mixture and in the ice I_h phase:

$$\mu_w^{\text{liq}}(T, P^{\text{atm}}, x) = \mu_w^{\text{ice}}(T, P^{\text{atm}}), \tag{4}$$

where P^{atm} is the atmospheric pressure and x is the mole fraction of alcohol in the liquid mixture. The thermodynamic algorithms related to phase equilibrium were solved by using the in-house thermodynamic framework presented in Refs. [59].

3.3. Heterogeneous nucleation theory for predicting the solid-formation temperature

In liquid mixtures below the saturation temperature, solid clusters form and dissipate continuously by means of thermal fluctuations. Nucleation occurs when a cluster permanently exceeds the critical size, R_c, after which further growth is spontaneous. If the critical cluster forms on the container walls or on the fiber, it is referred to as heterogeneous nucleation. If it forms in the bulk of the fluid, it is referred to as homogeneous nucleation. Spontaneous growth of the cluster occurs when the energy reduction of increasing the volume exceeds the energy cost of increasing the surface area. The rate of nucleation events can be expressed by the Arrhenius equation

$$J = J_{\text{kin}} \exp\left(-\frac{W}{k_B T}\right), \tag{5}$$

where the kinetic prefactor, J_{kin}, describes the rate of cluster formation in the absence of a thermodynamic free energy barrier. For heterogeneous nucleation on a wall, the nucleation rate scales linearly with the wall area, and the units of J are therefore [particles/m^{2}s]. The exponential factor captures how the rate is limited by the nucleation barrier, given by the work of formation, W, required to create clusters large enough to grow spontaneously. For heterogeneous nucleation, the work of formation can be written as [15,60].

$$W = f_{\text{het}} W^{\text{hom}}, \tag{6}$$

where W^{hom} is the corresponding work of formation for homogeneous nucleation, and f_{het} is the heterogeneity factor. The value of f_{het} depends on the surface topology of the container as well as the difference in surface energies of the container−liquid and the container−ice interfaces [15]. These surface energies are non-trivial to estimate. In this work, we assume f_{het} to be temperature-independent, concentration-independent, and equal to that of *pure* water in the given container. The heterogeneity factor is thus assumed to depend only on the container type. The quality of this assumption will be discussed in Sec. 4.

We assume the nucleation process to be isothermal. This is usually a good assumption, even for condensation from dense water + alcohol vapors [56,57], for which the latent heat for phase change is larger and the cooling rate of nuclei is likely lower than for crystallization. Furthermore, a recent simulation study also found that the dynamics of ice growth is not affected by heat dissipation [61].

We next describe how to calculate J_{kin} and W. For convenience we have also included a flowchart of the calculation procedure in Fig. 3.

The work of formation for homogeneous crystallization in *pure* water is given by [15].

$$W^{\text{hom}} = -\Delta P V_c + A_c \sigma_{i,w}, \tag{7}$$

where $V_c = 4\pi R_c^3/3$ and $A_c = 4\pi R_c^2$ are the volume and surface area of the critical ice cluster. The critical cluster is assumed to be spherical, with the radius given by the Young−Laplace equation

$$R_c = \frac{2\sigma_{i,w}}{\Delta P}. \tag{8}$$

Here, $\sigma_{i,w}$ is the surface energy between the ice and the liquid water, and ΔP is the pressure difference between the interior of the critical cluster and the surrounding liquid. The surface energy

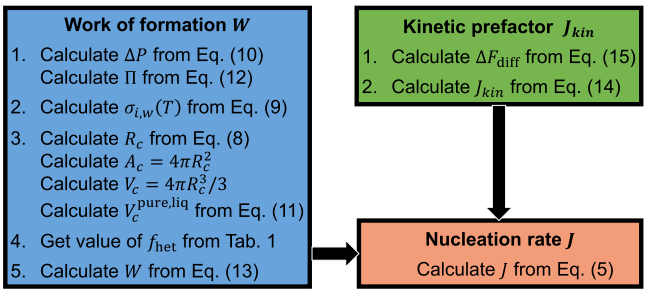

Fig. 3. Flowchart of the calculation procedure to obtain the nucleation rate.

depends on R_c [62], which in the theoretical framework is a unique function of T. In this work, we assume that the surface energy of the critical ice crystal depends linearly on temperature as

$$\sigma_{i/w}(T) = \sigma_{i/w}(T_0) + a(T - T_0), \tag{9}$$

where $T_0 = 273.15$ K. Following previous works [63,64], we use the values $\sigma_{i/w}(T_0) = 29.1$ mN/m, and $a = 0.2$ mN/(K m). We assume the surface energy to be independent of the crystal plane, which is a reasonable approximation for water according to Espinosa et al. [65].

The critical ice cluster has the same chemical potential as the water in the liquid phase, but will be at a higher pressure due to the Young–Laplace equation (Eq. (8)). For a given supercooled liquid mixture at temperature $T < T_{\text{melt}}$, the pressure increase ΔP of the critical cluster is found by solving for equality of chemical potentials of water in the two phases:

$$\mu_w^{\text{liq}}(T, P^{\text{atm}}, x) = \mu_w^{\text{ice}}(T, P^{\text{atm}} + \Delta P), \tag{10}$$

3.3.1. The heterogeneous nucleation barrier

The formation of solids will in most cases be catalysed by the container surface, where the container–liquid interaction reduces the nucleation barrier. The magnitude of the reduction depends on both the surface topology and the hydrophobicity of the container surface [19].

To estimate the work of formation is a crucial step of crystallization theory [63]. Since the work of formation is a difference between two state functions, it can be calculated by adding up free energy differences along any path between the initial and end states. A convenient path through the thermodynamic state space from the liquid mixture (initial state) to the critical cluster (end state) can be described as follows:

(a) Remove all alcohol molecules from the volume $V_c^{\text{pure,liq}}$ occupied by the number of water molecules that will be in the critical ice cluster.
(b) Form ice from the pure, supercooled water. The energy of Step (b) corresponds to the work of formation of a critical cluster of ice in supercooled, pure water.
(c) Re-equilibrate the ice crystal with the solution.

The energy difference of Step (a) is given by $\Pi V_c^{\text{pure,liq}}$ [64,66], where $\Pi > 0$ is the osmotic pressure across a membrane that is semipermeable to water and that encloses a volume, given by $V_c^{\text{pure,liq}}$ of pure water. The volume that is cleared from alcohol molecules in Step (a) is given by

$$V_c^{\text{pure,liq}} = V_c v_w^{\text{pure,liq}} \big/ v^{\text{ice}}, \tag{11}$$

where $v_w^{\text{pure,liq}}$ and v^{ice} are the molar volumes of pure water and ice, respectively. These were computed from the two EoS described in Sec. 3.1, at the supercooled state temperature T. The osmotic pressure Π was computed by identifying the pressure of pure water that gives the same chemical potential as the chemical potential of water in the liquid mixture, the latter being at atmospheric pressure:

$$\mu_w^{\text{liq}}(T, P^{\text{atm}} - \Pi, 0) = \mu_w^{\text{liq}}(T, P^{\text{atm}}, x). \tag{12}$$

The energy difference of Step (b) is given by the usual expression for the work of formation for a critical cluster of ice in pure water (Eq. (7)). The energy difference of Step (c) was assumed to be small compared to the energy differences of Steps (a) and (b) and hence omitted; although this is a common approach in the literature [64,66], the quality of this approximation is unknown.

The final expression for the work of formation is thus

$$W = \left(\Pi V_c^{\text{pure,liq}} - (\Delta P) V_c + A_c \sigma_{i,w}\right) f_{\text{het}}, \tag{13}$$

where V_c, A_c and $\sigma_{i/w}$ are computed by using Eqs. (8) and (9), and ΔP is given by the condition of equal chemical potential of water in the liquid solution (at atmospheric pressure P_{atm}), and in the ice (at pressure $P_{\text{atm}} + \Delta P$).

3.3.2. The kinetic prefactor and ice growth

The kinetic prefactor in Eq. (5) describes the rate of diffusion across the solid–liquid interface, and is modeled by [67]

$$J_{\text{kin}} = N_c \frac{k_B T}{h} \exp\left[-\frac{\Delta F_{\text{diff}}}{k_B T}\right] \tag{14}$$

In Eq. (14), h is Planck's constant, N_c is the number of water molecules in contact with the container wall per unit area, and ΔF_{diff} is the activation energy for transport across the surface of the critical cluster. In pure water, this activation energy can be estimated [60] by relating it to the self-diffusivity $D(T)$ of water as $\Delta F_{\text{diff}} = (\partial, \ln, D(T)/\partial T) k_B T^2$. Although the self-diffusivity in water is usually lower in alcohol–water mixtures than in pure water, we will approximate it by its value in pure water. We numerically verified that this did not significantly alter the predictions of the solid-formation temperature: for the ethanol–water mixture, we found that a 50% increase in the activation energy for diffusion of water lowers the supercool limit by less than 1 K.

For pure water, we used the value $N_c = 5.85 \times 10^{18}$ m^{-2} [63,67]. In mixtures, this was multiplied by the mole fraction of water. The activation energy for transport across the surface was estimated following Zobrist et al. [60]:

$$\Delta F_{\text{diff}}(T) = \frac{k_B T^2 E}{(T - T_0)^2}, \tag{15}$$

where the values $T_0 = 118$ K and $E = 892$ K were taken from Smith and Kay [68].

The self-diffusion of water affects the rate of crystal growth, $u(T)$ [m/s], which is a function of temperature. This can be estimated with Wilson–Frenkel theory [61,69]:

$$u(T) = \frac{D(T)}{a}\left[1 - \exp\left(-\frac{|\Delta\mu_w(T)|}{k_B T}\right)\right], \tag{16}$$

where $D(T)$ is the self-diffusion coefficient of water in the mixture, and a is a characteristic length scale on the order of the diameter of a water molecule that was estimated as 3 Å, in accordance with Ref. [61]. Moreover, $\Delta\mu_w$ is the difference in chemical potential of water in the two phases, both at atmospheric pressure. The quantities in Eq. (16) are evaluated at the solid-formation temperature, T. Although freezing of ice is an exothermic process, molecular simulations indicate that the heat is dissipated sufficiently fast so as to not impact the growth dynamics [61].

3.3.3. The solid-formation temperature

Once the nucleation barrier and the kinetic prefactor have been estimated, the nucleation rate can be calculated from Eq. (5). However, to set a specific limit for a supercooling temperature when the solid forms, one must decide on a *critical* nucleation rate that represents the observed sudden phase change. The critical nucleation rate must be chosen with the cooling rate in mind. In this work, we have used that $\overline{N}_{\text{crit}} = 1\ \text{s}^{-1}$, where $\overline{N}_{\text{crit}}$ denotes the rate at which critical clusters are formed. Given a value for $\overline{N}_{\text{crit}}$, we find the solid formation temperature by solving

$$J(T)A_{\text{container}} = \overline{N}_{\text{crit}}, \tag{17}$$

where $A_{\text{container}} \approx 0.001\ \text{m}^2$ is the wetted area of the container. Similar to the superheating temperatures determined in Refs. [30], the exact value of $\overline{N}_{\text{crit}}$ had a small influence on the prediction of the temperature where a sudden phase change occurs. We emphasize that $\overline{N}_{\text{crit}}$ does not represent the actual experimental rate. Since the exact value for $\overline{N}_{\text{crit}}$ has a small influence on the predicted solid-formation temperature, we need to ensure that $\overline{N}_{\text{crit}}$ is similar to the experimental nucleation rates. This is true for $\overline{N}_{\text{crit}} = 1\ \text{s}^{-1}$, since 1 s is a characteristic time scale that is low compared to the cooling rate, but high enough to expect a nucleation event on the time-scale of the solid-formation detection.

3.4. Latent heat of solid-formation

The latent heat released during ice formation limits the amount of ice that can be produced without additional heat dissipating out of the container. Immediately after the solid formation, the system can be approximated to be adiabatic. This allows the amount of ice to be estimated with the following energy balance:

$$C_p^{\text{liq}} m_{\text{liq}} \Delta T_s + C_p^{\text{ice}} m_{\text{ice}} \Delta T_s = \Delta H_{\text{fus}}^{\text{ice}} m_{\text{ice}}, \tag{18}$$

where m_{ice} is the ice mass, m_{liq} is the remaining liquid, C_p^{liq} and C_p^{ice} are the specific heat capacities of the liquid and ice, ΔT_s is the supercooling, and $\Delta H_{\text{fus}}^{\text{ice}}$ is the enthalpy of fusion for ice.

4. Results and discussion

In the following, we will first discuss the experimental methodology (Sec. 4.1). Next, the influence of container material and fluid mixture (Sec. 4.2) on the solid-formation temperature will be evaluated by comparing the experiments to theoretical predictions. The growth rate of the crystal posterior to the solid-formation will be discussed (Sec. 4.3), before further remarks on the heterogeneous nucleation theory are given (Sec. 4.4). Binary water−alcohol mixtures containing methanol, ethanol, 1-propanol and 1-butanol will be considered. A minimum of four solid-formation events have been detected for each experimental point reported. For all experiments, a visual inspection confirmed that the solid-formation started at the container walls and not on the two sensor probes.

4.1. Experimental determination of the solid-formation temperature

The sensors were placed in a container with a 6 mL liquid sample according to the setup depicted in Fig. 1. The container was cooled down to − 30°C at a rate of 0.2 °C/min. The acquisition parameters and data processing was carried out as described in Section 2.2. Fig. 4 shows how the wavelengths shift for the two sensor types in a water-mixture with 9 mol% methanol during cooling, upon freezing, and during further cooling of the frozen solid.

Both sensors shift towards shorter wavelengths (blue-shift) as the temperature is decreased. The non-linear thermo-optic properties of the liquid phase give a non-linear response for the thin-core (TC) sensor, as depicted in Fig. 4-top. The responses from the two sensors in the liquid phase can be used to create a baseline, or a calibration curve. Any deviation from this behavior indicates a change in the properties of the sample, which in these experiments can be interpreted as the phase transition. This was further confirmed with the boroscope, which was used to visually monitor the sample.

Upon freezing, both sensors exhibit a sudden red-shift, i.e. a shift to longer wavelengths. This is attributed to the release of latent heat during freezing, which heats the sample. Because the solid phase consists of pure ice both for pure water and the binary mixtures, the concentration of the remaining liquid phase will increase during freezing. The temperature of a mixture during solid formation will thus proceed along a continuously decreasing curve.

Eventually, the freezing process slows down and the sample recovers a tight thermal match with the temperature bath, which can be seen by the wavelength of the Fiber-Bragg-Grating (FBG) sensor resuming a linear behavior, as shown in Fig. 4-bottom. However, the TC wavelength remains at a longer wavelength, also after the freezing process has completed. Because the sample temperature is now nearly equal to that of the temperature bath, this shift is attributed to an increase in the refractive index (RI) around the TC sensor. Pure ice has a lower RI than the liquid mixtures, and the increased RI is therefore assumed to be caused by the increased concentration of the remaining liquid phase surrounding the sensor. For pure water, the expected blue-shift is observed after freezing.

In summary, the combined output from the two sensors gives unique information on both the initiation and the progression of the phase transition. Because of the slow cooling rate and frequent acquisition, the freezing points can be detected with an uncertainty limited by the accuracy of the temperature bath (0.25 K).

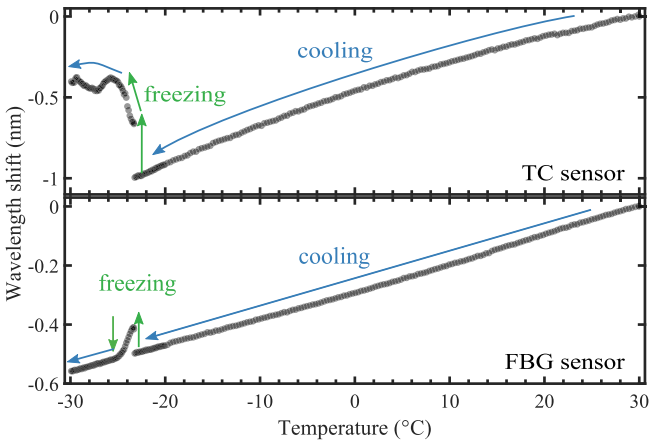

Fig. 4. Wavelength shifts from the TC sensor (top) and the FBG sensor (bottom) as a function of temperature for a water−methanol mixture with 9 mol% methanol. The solid-formation event is indicated for both sensors.

4.2. Solid-formation temperatures in water–alcohol mixtures

In order to compare the experimental results to the predictions from the theory presented in Sec. 3, it is first necessary to determine the heterogeneity factor in Eq. (6). The heterogeneity factor was determined by reproducing the experimental solid-formation temperature of pure water by using the heterogeneous nucleation model presented in Sec. 3. We find that the value of f_{het} depends on the container material. The resulting values have been tabulated in Table 1. These values are in agreement with previous work by Zobrist et al. [60], who found hetereogeneity factors between 0.02 and 0.26 for nucleation on a nonadecanol surface. With the heterogeneity factor at hand, the theoretical model is fully predictive for the solid-formation temperatures of alcohol–water mixtures.

4.2.1. The influence of container type and cleaning procedure on the solid-formation temperature

To investigate the influence of container-type and experimental methodology on the solid-formation temperature, a series of tests was carried out with water-ethanol mixtures in two different container types, glass and poly-propylene (PP).

Fig. 5 shows that the solid-formation temperatures in new, untreated PP are lower than the corresponding temperatures in glass. PP is a highly hydrophobic material because of the long aliphatic polymer chains, and thus less wetting than glass. This is reflected in a significantly higher value for the heterogeneity factor (see Table 1).

The experimental protocol outlined in Sec. 2.3 involves cleaning the containers with both acetone and ethanol between the experiments in order to remove impurities. The same glass test tube was used for all experiments, and this procedure was found to give the most reproducible results. For the PP test tubes, a new, sterile test tube was used for each measurement. Further experiments were conducted with these to gain insight into the difference between the pristine and cleaned surfaces with regards to the solid-formation temperature.

The sterile PP surface gave solid-formation temperatures that were on average 5–6 °C below those in glass. The cleaned PP surfaces still gave lower solid-formation temperatures than glass, as shown in Fig. 5, but less so than the sterile PP. Furthermore, the effect of cleaning the PP depended on the concentration of ethanol in the mixture. The 8.9 mol% ethanol did not freeze consistently and the point in the graph represents only one measurement. The almost constant difference between the sterile test tubes and the glass indicates that the cleaning procedure outlined in Sec. 2 is well suited for glass, but not for PP.

Cleaning the container with only acetone did not raise the solid-formation temperature to the same degree as using both acetone and ethanol. Hence, a possible explanation for the change in the solid-formation temperature is that ethanol molecules adsorb on the PP container wall and in this way enhances the surface interaction between the PP container wall and the ice due to increased hydrophilicity. This seems to be in contradiction to the findings by Wu et al. [70], who investigated the effect of varying the density of OH-groups in polyvinyl alcohols on heterogeneous nucleation [70]. The increased hydrophobicity with less OH-groups was argued to pose less of a constraint on the interfacial water molecules and lead to more efficient nucleation. We emphasize that heterogeneous nucleation is a complex phenomenon, where the solid-formation depends on many parameters in addition to the hydrophobicity of the container wall.

Table 1
Values of the heterogeneity factor, f_{het} for the container materials considered in this work.

Material	Value
Glass	0.12
Polypropylene (new)	0.25

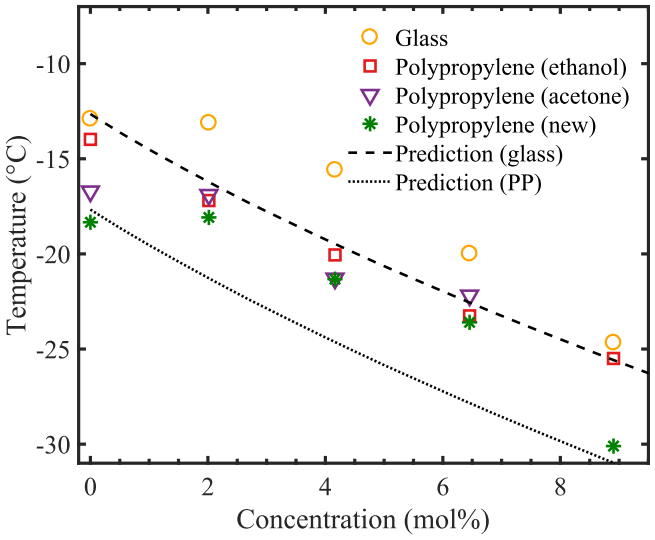

Fig. 5. Comparison of ethanol–water solid-formation temperatures for glass and polypropylene test tubes, new sterile tubes or cleaned with acetone or ethanol.

4.2.2. The influence of the cooling-rate and the experimental set-up on the solid-formation temperature

Theoretically, any temperature below the melting temperature will cause a nucleation event, provided enough time i.e. with an infinitely slow cooling rate. Hence, increasing the cooling rate will result in a lower freezing temperature, as was shown by Koga et al. [32]. Koga et al. used significantly higher cooling rates than us of 5, 10 and 20 °C/min. Although no systematic study was carried out in this work to investigate the influence of the cooling rate, we did not find any change in the solid-formation temperature with moderate changes (0.1 and 0.3 °C/min). In the theory presented in Sec. 3.3, the critical nucleation rate that was chosen represents a characteristic time-scale for solid formation. Since the critical nucleation rate was found to have a small influence on the predicted solid-formation temperature, this further supports that the solid-formation temperature should be rather insensitive to the cooling rate.

The fiber-optic sensors may influence the solid formation temperature if their surfaces are better nucleating agents than the container. However, from the videos captured with the boroscope, we can deduce that the crystal forms at the container wall. This would be the same for other methods used – if they affect the conditions in the sample, the solid formation temperature could be different. Since the nucleation event occurs on the container surface, there will be some delay before the sensors will be able to detect the phase-transition. The measurements indicate that the delay in the current setup depends on the crystal growth rate, which decides how early the conditions around the sensors change in response to the new phase.

4.2.3. Results for binary water–alcohol mixtures

Fig. 6 compares the theoretical predictions from Sec. 2 to experimentally determined solid-formation and melting temperatures of ice in four binary water–alcohol mixtures. Only glass containers have been used in these experiments. The experimentally determined solid-formation temperatures are summarized in Table 2, and the complete data set is available in the SI.

As expected when dealing with heterogeneous nucleation, a few of the experiments gave significantly higher solid-formation temperatures than the trend. Although utmost care was taken to ensure a clean environment and pure samples, this was assumed to be caused by contaminants acting as nucleating agents [71]. When the experiments were repeated, the samples gave a solid-formation temperature in vicinity of the trend-line, which is interpreted as heterogeneous nucleation on the glass-liquid interface. However, for the pure water samples, a larger dispersion of freezing temperatures was observed. A possible explanation for this may be the absence of alcohol molecules in the solution that otherwise may adsorb on the glass surface. In pure water, the process is reversed as desorption of the ethanol and acetone molecules left from the cleaning stage may occur. This process may be less predictable and hence cause the larger dispersion. A large dispersion in solid formation temperatures is also seen for the 7.5 wt% butanol sample. This is close to the solubility limit for butanol (7.7 wt% at 20 °C) and may therefore be caused by partial phase separation as the sample is cooled down.

Experiments were conducted with at least two different samples for each concentration. The samples were drawn from the same mixture reservoir and should therefore have the same concentrations. For each concentration, the samples were cooled to the freezing point a total of minimum three times (see SI for further details). The data for 0% (i.e. pure water) is the same for each binary mixture. To avoid systematic errors in the detected solid-formation temperatures, the measurement sequence was performed both with increasing and decreasing concentrations.

The experimentally determined melting temperatures of ice in binary water–alcohol mixtures with methanol [72], ethanol [72], 1-propanol [73] and 1-butanol [74] are reproduced to a reasonable accuracy by the CPA + Ice model described in Sec. 3.2. At higher alcohol concentrations, the model predictions give melting temperatures that lie above the tabulated values. While the melting temperatures from the theory follow a close to linear trend as a function of the alcohol concentration, the tabulated experimental values are more parabolic. To gain further insight into this difference, we performed a sensitivity analysis of the CPA + Ice model. Changing the parameters of the ice model had a minor influence on the predicted melting points. In particular, it did not result in a non-linear curve for the melting points. A more accurate EoS for the water–alcohol mixtures than CPA is probably needed to improve the agreement between the experimental and predicted melting points. Although CPA predicts the vapor–liquid coexistence accurately, it can exhibit appreciable deviations for enthalpies of fusions, as shown for ethanol–water mixtures in the SI.

The solid-formation temperatures decrease with alcohol concentration, as shown in Fig. 6, and follow a similar trend as the melting temperatures. The degree of supercooling, shown in Fig. 7, varies between 11 K and 17 K. Unlike the solid-formation temperatures, the degree of supercooling has a much more curious behavior. For the mixtures with the alcohols of shortest chain-

Table 2
Solid-formation temperatures in a glass test tube. The mean temperatures are given, with the largest standard deviation of 2.2 °C.

Concentration (weight):	0%	5%	10%	15%	20%
Methanol (°C):	−12.8	−15.0	−19.0	−22.8	−29.2
Ethanol (°C):	−12.8	−13.1	−15.6	−20.0	−24.6
Propanol (°C):	−12.8	−15.5	−17.6	−22.4	−25.0
Butanol (°C):	−12.8	−17.6	–	–	–

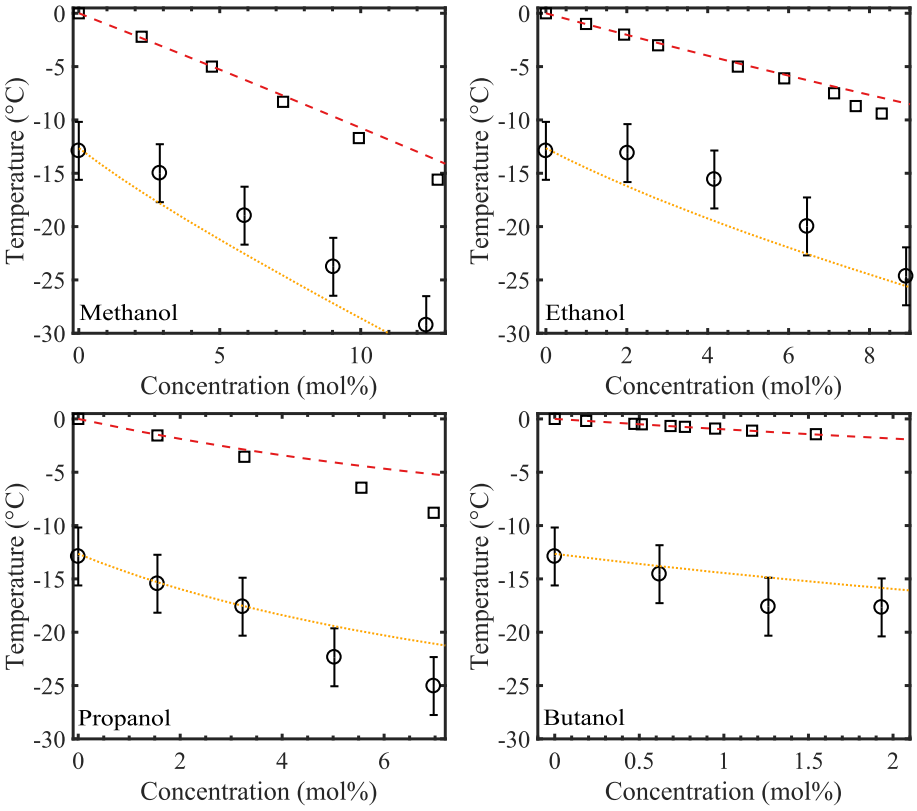

Fig. 6. Plot of the experimental solid-formation temperatures (circles) for methanol, ethanol, 1-propanol and 1-butanol. Melting temperatures (squares) from Ref. [72] (methanol, ethanol) [73] (1-propanol) and [74] (1-butanol). The predicted freezing and melting temperatures are shown in dotted-yellow and dashed-red, respectively. Error bars include the measurement spread and the temperature bath accuracy.

length, methanol and ethanol, the degree of supercooling displays a dip at the lowest concentrations, before it increases at higher concentrations. Within the uncertainty of the measurements, the supercooling of the mixtures with propanol and butanol appears to increase with alcohol concentration. The predictions from the heterogeneous nucleation model presented in Sec. 3.3 display qualitatively different trends than the experimental data. This creates a systematic deviation between the experiments and the predictions shown in Fig. 8, which varies from a 4 K overprediction for water-ethanol to a −3 K underprediction for water−butanol.

In the theoretical predictions, the degree of supercooling is to a good approximation a colligative property with alcohol mole percentages below about four, i.e. it depends only on the number of alcohol solute molecules. This may stem from the osmotic pressure entering the heterogeneous nucleation theory (Sec. 3.3). We found that the osmotic contribution from the term ΠV_c can be a large fraction of W, in some cases constituting 60% of the work of formation. For the low concentrations of alcohol considered here, the osmotic pressure Π is to a large extent a colligative property; indeed, it is well-approximated by $\Pi = \rho_{\text{alc}} k_B T$ where ρ_{alc} is the alcohol density. We found that including the osmotic contribution was key to obtain a supercooling temperature that increases with alcohol concentration.

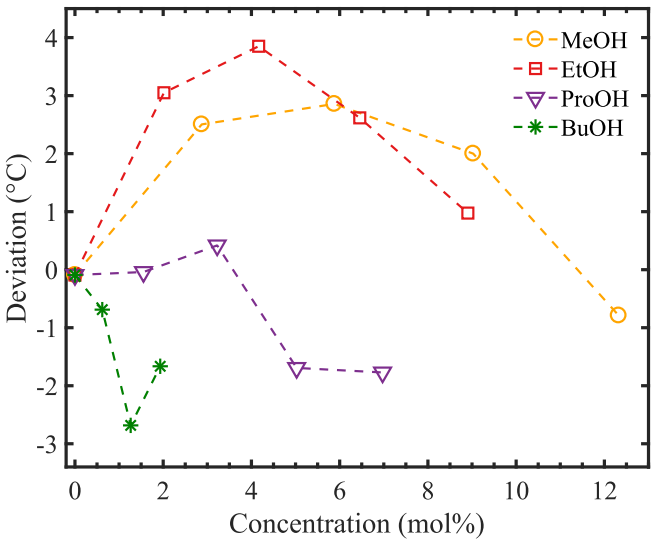

Fig. 8. Deviation between measured solid-formation temperatures and predictions from heterogeneous nucleation theory.

4.3. The kinetic prefactor and crystal growth

We showed in Sec. 4.2 that there is a qualitative difference between the measured values and the theoretical predictions of the solid-formation temperature in binary water−alcohol mixtures. In Sec. 3.3.2, we explained that the kinetic prefactor was proportional to the self-diffusion coefficient of water. This coefficient can be linked to the growth velocity of an ice crystal by use of Wilson−Frenkel theory (Eq. (16)). In the following, we will investigate whether a poor description of the kinetic prefactor in the theory can be the cause of the deviation between theory and experiments.

A boroscope combined with video-recording and a careful post-processing enabled us to estimate the growth rate of ice crystals formed in water-ethanol mixtures at several compositions. The propagation length of the ice front as a function of time is shown in Fig. 9. The figure shows that the growth is close to linear, and the proportionality factor gives an approximately constant growth rate. Images of the crystal growth progress can be found in the SI.

Table 3 reports the growth rates of crystals forming in different ethanol−water mixtures. The growth rate in pure water was found to be 10.2 cm/s. It was found to be in the range 0.9−1.24 mm/s for 4.2 mol% ethanol (10 wt%), and to be 0.25 mm/s for 11.5 mol% ethanol (25 wt%). After 0.8 s, the mass of ice produced was estimated to be approximately $1.1 \cdot 10^{-4}$ g and $2.5 \cdot 10^{-5}$ g for 4.2 mol% and 11.5 mol%, respectively. From these numbers, one can infer that the concentration in the remaining liquid phase remains essentially unchanged at this stage of the phase transition. Furthermore, the amount of ice formed during the investigation of the growth is much lower than the amount of ice that can be produced (∼0.9 g) with the amount of supercooling achieved in the measurements, as estimated by Eq. (18). The crystal growth should therefore not be limited by the rate of heat transfer out of the test tube this early in the freezing process. These findings are in agreement with the work in Refs. [61], where it was shown that the crystal growth in pure water does not depend on heat dissipation in the early stages of the phase transition. This explains the nearly constant growth rates observed in the experiments.

For pure water, a crystal growth rate of 10.2 cm/s at 16 K supercooling is in excellent agreement with previous experimental studies [75−77]. The crystal growth retardation observed for the ethanol mixtures however, is one order of magnitude larger than what was found in freezing of aqueous NaCl solutions [77]. In a solution with 5 mol% NaCl (10 mol% dissociated, 14.6 wt%), the ice had a growth rate of 4 mm/s [77]. The higher growth rates in NaCl may be caused by a larger hydration shell around the ethanol

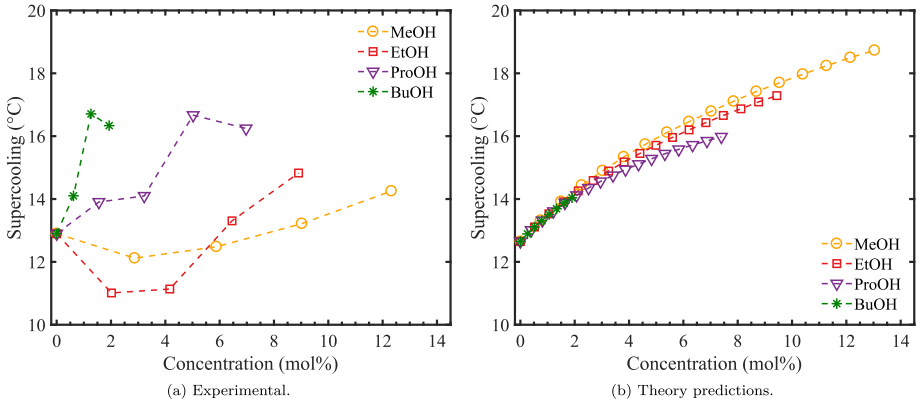

Fig. 7. Comparison of the degree of achieved supercooling before solid formation for the water−alcohol mixtures from experiments (a) and predictions from theory (b).

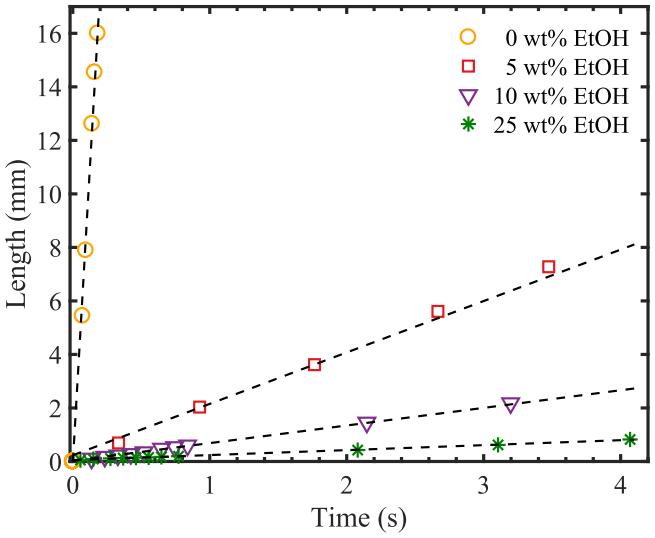

Fig. 9. Propagation distance of the crystal surface during growth as a function of time. The curves are extrapolated to the expected time of the nucleation, set to zero. For pure water, the ice reaches the opposite side of the 16 mm inner diameter test tube after 0.18 s, which gives an average growth rate of 10.2 cm/s (linear fit). The unidirectional growth rates for the approximately spherical crystals in the ethanol mixtures are 0.9 mm/s and 0.25 mm/s for 4.2 mol% (10 wt%) and 11.5 mol% (25 wt%) ethanol, respectively.

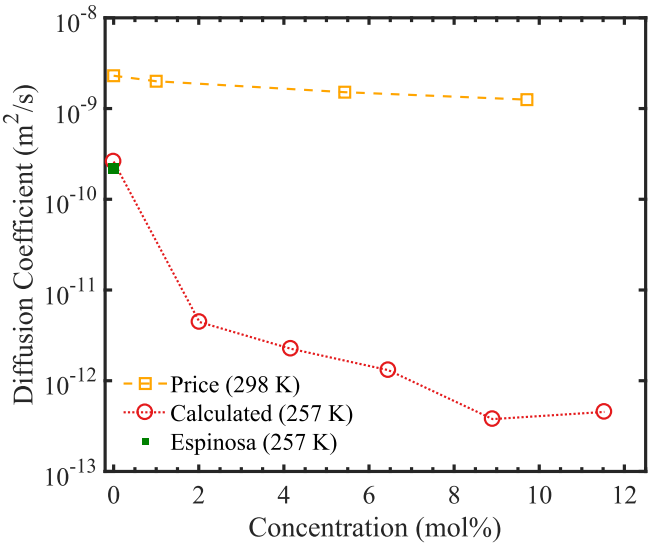

Fig. 10. Diffusion coefficients calculated from combining Wilson–Frenkel theory (Eq. (16)) with measured growth rates (Table 3), calculated chemical potentials and the radius ($a = 3$ Å) from de Hijes [61], together with values from Espinosa et al. (2016) [79] estimated at the same temperature (−16.2 °C) and from Price et al. (2003) at 25 °C [78].

molecules than the NaCl ions, which impedes the diffusion of water molecules. The slower crystal growth has been hypothesized to be because of the required diffusion of solute molecules away from the ice front, which is slower in more concentrated solutions [78].

To shed further light on the concentration dependence of the growth rate, we have used the Wilson–Frenkel theory [61,69] in Eq. (16) with $\mu_w(T)$ computed by the CPA EoS to estimate an *effective* diffusion coefficient based on the experimentally determined growth rates. The effective diffusion coefficient plotted in Fig. 10 drops three orders of magnitude with addition of only 9 mol percent ethanol. This is in contrast to the experimentally determined self-diffusion coefficient of water in water–ethanol mixtures from Price et al. [78], which is reduced by a factor of two in the same interval due to the concentration dependence (see results at 298 K in Fig. 10). The reduced solid-formation temperature at higher alcohol concentrations is also expected to decrease the diffusion coefficient, although not to the extent displayed by the effective diffusion coefficient in Fig. 10.

For pure water, the self-diffusion coefficient obtained by the measured growth rates is in excellent agreement with the experimentally determined self-diffusion coefficient at 260 K, as shown in the figure. The large drop in the effective diffusion coefficient from Wilson–Frenkel theory with increasing ethanol concentrations probably points towards other effects than self-diffusion being important, such as accumulation of ethanol molecules at the interface of the growing crystal. It is unclear whether such accumulation is as important for the critical cluster, as for the macroscopic crystals observed in the boroscope. Nonetheless, we have investigated the impact of replacing the self-diffusion coefficient used as input in Eq. (14) by that inferred by combining Wilson–Frenkel theory with the measured growth rates. This changes the predicted solid-formation temperature by less than 1 K, hence it cannot explain the systematic deviations between theory and predictions for the solid-formation temperature.

Table 3
Crystal growth rates for different concentrations of ethanol. Two measurements were performed for the concentrations 5 wt% and 10 wt%. The freezing temperatures are shown in parenthesis.

0 wt%	5 wt%	10 wt%	15 wt%	20 wt%	25 wt%
10.2 cm/s (-16.2 °C)	1.9 mm/s (-12.4 °C) 2.0 mm/s (-12.2 °C)	0.9 mm/s (-17.4 °C) 1.24 mm/s (-17.1 °C)	0.66 mm/s (-19.9 °C)	0.20 mm/s (-25.3 °C)	0.25 mm/s (-26.3 °C)

4.4. Further discussion of heterogeneous nucleation theory

To gain further insight into the origin of the discrepancy between the experiments and the predictions, we have carried out a comprehensive sensitivity analysis of the different components of the heterogeneous nucleation model presented in Sec. 3.3.

The onset nucleation rate of 1 critical cluster per second used in Eq. (17) was chosen somewhat arbitrarily. We tested this choice by increasing and decreasing $\overline{N}_{\text{crit}}$ by a factor 1000. This changed the supercooling temperatures by less than 1 K. Hence, the exact choice of this parameter is not crucial for the theory.

We also tested the impact of varying the ice–water surface energy $\sigma_{i/w}$ by ±20%. Although this shifted the solid-formation temperature, it did not shift the trend.

Many of the assumptions in constructing the thermodynamic route to compute the activation barrier of ice in water-alcohol mixtures are questionable. For instance, the re-equilibration of the ice crystal (step c) with the solution has been neglected. For step (a), Warkentin et al. [66] argued that the volume that needs to be cleared of water molecules should include an extra shell equal to the Stokes radius of the solute (i.e., the alcohol), but we found that this has negligible influence on the predicted solid-formation temperatures. We also found that using V_c instead of $V_c^{\text{pure,liq}}$ for estimating the work of formation (Eq. (13)) had negligible effect on the solid-formation temperatures.

Another possible reason for the discrepancy between the theoretical predictions and the measurements is the assumption that the heterogeneity factor, f_{het}, was assumed to be constant and equal to that of pure water. It follows from the expression (6) for the

work of formation that, for each experiment, one can fit f_{het} to obtain a perfect match with the theory. For the glass container, we find that all experiments can be fitted in this way by varying f_{het} in the narrow interval 0.09–0.15. An important topic for future work in heterogeneous nucleation theory is therefore to develop a more reliable model for f_{het} for binary mixtures, which incorporates a dependence on both the alcohol type and composition.

Some of the deviations between the predicted solid-formation temperature and the measurements, e.g. for propanol, display a similar behavior as the misprediction of the melting temperature. Since the melting temperature is independent of the nucleation barrier, it seems reasonable that part of the deviations can be attributed to inaccuracies in the CPA + Ice model for the bulk thermodynamics.

5. Conclusion

In this work, we have investigated by theory and experiments the solid-formation and the melting temperature of ice in four binary water–alcohol mixtures containing methanol, ethanol, propanol and butanol.

A dual fiber-optic sensor set-up was used to obtain the solid-formation temperature. The solid-formation was detected by measuring a change in the refractive index of the sample and an increase in the local temperature due to the release of latent heat. The two sensors could independently detect the phase transition, but they could also be used for further analysis of the phase transition when combined. The growth rate of the ice crystal after formation was determined experimentally by use of a boroscope, video-recording and a careful post-processing analysis.

The predictions from the CPA equation of state combined with a model for pure ice were in good agreement with experimental results for the melting temperatures of binary water-alcohol mixtures. However, the theory over-predicted the melting points at higher alcohol concentrations. This was attributed to inaccuracies in the CPA equation of state.

Experiments with water–ethanol mixtures were conducted both in glass and polypropylene containers, where the latter exhibited a higher degree supercooling, amounting to 5–6 °C. This was explained by the lower hydrophilicity of polypropylene. After exposing the polypropylene to pure ethanol in the cleaning procedure, the solid-formation temperature permanently increased. A possible explanation for this is that ethanol molecule adsorb on the wall and in the material of the container. No similar behavior could be observed for the glass containers, which were used in the remaining part of the experiments.

The solid-formation temperatures were shown to decrease with alcohol concentration, and followed a similar trend as the melting temperatures. The degree of supercooling varied between 11 K and 17 K and displayed a highly non-linear dependence on the alcohol concentration. For the mixtures with methanol and ethanol, the degree of supercooling displayed a dip at the lowest concentrations, before it increased at higher concentrations. The supercooling of the mixtures with propanol and butanol increased with the alcohol concentration.

A heterogeneous nucleation model was developed to predict the solid-formation temperatures of the binary alcohol–water mixtures. The predictions from this model displayed qualitatively different trends than the experimental data. A systematic deviation between the experiments and the predictions was observed, varying from a 4 K overprediction for water–ethanol to − 3 K underprediction for water–butanol. The model predicted the degree of supercooling to be, to a good approximation, a colligative property. This was not in agreement with the experimental results, and sensitivity analyses pointed to inaccuracies in the work of formation as a likely reason for the deviations. Perhaps the crudest assumption in the theory was that the heterogeneity factor is independent of concentration, and a dependence on composition and mixture type may be necessary to improve the predictions.

For pure water, crystal growth rates of 10.2 cm/s at 16 K supercooling were measured. These are in excellent agreement with previous results reported in the literature. The crystal growth rate observed in ethanol–water mixtures however, was much lower, where a crystal in a mixture with 4 mol% ethanol grew at a rate of 1 mm/s. The order-of-magnitude reduction in the growth rate with increasing ethanol concentration was hypothesized to result from accumulation of alcohol molecules at the crystal surface during the growth of the crystal.

CRediT authorship contribution statement

Markus Solberg Wahl: Conceptualization, Methodology, Software, Validation, Formal analysis, Investigation, Writing - original draft, Visualization. **Ailo Aasen:** Conceptualization, Methodology, Software, Validation, Formal analysis, Investigation, Writing - original draft, Visualization. **Dag Roar Hjelme:** Conceptualization, Methodology, Validation, Formal analysis, Investigation, Resources, Writing - review & editing, Supervision, Project administration, Funding acquisition. **Øivind Wilhelmsen:** Conceptualization, Methodology, Validation, Formal analysis, Investigation, Resources, Writing - original draft, Writing - review & editing, Supervision, Project administration, Funding acquisition.

Declaration of competing interest

The authors declare that they have no known competing financial interests or personal relationships that could have appeared to influence the work reported in this paper.

Acknowledgement

We thank Roger Aarvik for help during the experimental campaign. The work was supported in part by the strategic research funding from the Norwegian University of Science and Technology (NTNU), in part by the Interreg Sweden-Norway program (IR2015.01), and in part by the Energy and Sensor Systems group (ENERSENSE, strategic research program at NTNU).

Appendix A. Supplementary data

Supplementary data to this article can be found online at https://doi.org/10.1016/j.fluid.2020.112741.

References

[1] J. MacAdam, S.A. Parsons, Calcium carbonate scale formation and control, Rev. Environ. Sci. Biotechnol. 3 (2) (2004) 159–169, https://doi.org/10.1007/s11157-004-3849-1.

[2] M. Boerkamp, D.W. Lamb, P.G. Lye, Monitoring the kinetics of heterogeneous crystal growth using an intrinsic exposed core optical fibre sensor, Sensor. Actuator. B Chem. 240 (2017) 168–173, https://doi.org/10.1016/j.snb.2016.08.133.

[3] Ø. Wilhelmsen, D. Berstad, A. Aasen, P. Nekså, G. Skaugen, Reducing the exergy destruction in the cryogenic heat exchangers of hydrogen liquefaction processes, Int. J. Hydrogen Energy 43 (10) (2018) 5033–5047, https://doi.org/10.1016/j.ijhydene.2018.01.094.

[4] L. Zhang, Solid-fluid Phase Equilibria for Natural Gas Processing at Low Temperatures, Ph.D. thesis, Norwegian University of Science and Technology, Department of Energy and Process Engineering, 2012.

[5] B. Tohidi, A. Chapoy, J. Yang, Developing a hydrate-monitoring system, SPE Projects, Facilities Constr. 4 (2009) 1–6, https://doi.org/10.2118/125130-PA, 01.

[6] M. Tuinier, M. van Sint Annaland, G. Kramer, J. Kuipers, Cryogenic CO2 capture using dynamically operated packed beds, Chem. Eng. Sci. 65 (1) (2010)

114–119, https://doi.org/10.1016/j.ces.2009.01.055.
[7] A. Sharma, V.V. Tyagi, C.R. Chen, D. Buddhi, Review on thermal energy storage with phase change materials and applications, Renew. Sustain. Energy Rev. 13 (2) (2009) 318–345, https://doi.org/10.1016/j.rser.2007.10.005.
[8] F.G. Qin, A.B. Russell, X.D. Chen, L. Robertson, Ice fouling on a subcooled metal surface examined by thermo-response and electrical conductivity, J. Food Eng. 59 (4) (2003) 421–429, https://doi.org/10.1016/S0260-8774(03)00002-5.
[9] S. Veesler, L. Lafferrère, E. Garcia, C. Hoff, Phase transitions in supersaturated drug solution, Org. Process Res. Dev. 7 (6) (2003) 983–989, https://doi.org/10.1021/op034089f.
[10] D. Erdemir, A.Y. Lee, A.S. Myerson, Polymorph selection: the role of nucleation, crystal growth and molecular modeling, Curr. Opin. Drug Discov. Dev 10 (6) (2007) 746–755.
[11] J.R. Cox, L.A. Ferris, V.R. Thalladi, Selective growth of a stable drug polymorph by suppressing the nucleation of corresponding metastable polymorphs, Angew. Chem. Int. Ed. 46 (23) (2007) 4333–4336, https://doi.org/10.1002/anie.200605257.
[12] P. Mazur, Cryobiology: the freezing of biological systems, Science 168 (3934) (1970) 939–949, https://doi.org/10.1126/science.168.3934.939.
[13] A. Lintunen, T. Hölttä, M. Kulmala, Anatomical regulation of ice nucleation and cavitation helps trees to survive freezing and drought stress, Sci. Rep. 3 (2013) 2031, https://doi.org/10.1038/srep02031.
[14] D. Zaragotas, N.T. Liolios, E. Anastassopoulos, Supercooling, ice nucleation and crystal growth: a systematic study in plant samples, Cryobiology 72 (3) (2016) 239–243, https://doi.org/10.1016/j.cryobiol.2016.03.012.
[15] H. Vehkamäki, Classical Nucleation Theory in Multicomponent Systems, Springer Verlag, Berlin, 2006, https://doi.org/10.1007/3-540-31218-8.
[16] W.G. Finnegan, S.K. Chai, A new hypothesis for the mechanism of ice nucleation on wetted AgI and AgI.AgCl particulate aerosols, J. Atmos. Sci. 60 (14) (2003) 1723–1731, https://doi.org/10.1175/1520-0469(2003)060<1723:ANHFTM>2.0.CO;2.
[17] B.J. Murray, S. Broadley, T. Wilson, J. Atkinson, R. Wills, Heterogeneous freezing of water droplets containing kaolinite particles, Atmos. Chem. Phys. 11 (9) (2011) 4191–4207, https://doi.org/10.1039/c2cs35200a.
[18] B.J. Murray, D. O'Sullivan, J.D. Atkinson, M.E. Webb, Ice nucleation by particles immersed in supercooled cloud droplets, Chem. Soc. Rev. 41 (19) (2012) 6519–6554, https://doi.org/10.1039/c2cs35200a.
[19] M. Fitzner, G.C. Sosso, S.J. Cox, A. Michaelides, The many faces of heterogeneous ice nucleation: interplay between surface morphology and hydrophobicity, J. Am. Chem. Soc. 137 (42) (2015) 13658–13669, https://doi.org/10.1021/jacs.5b08748.
[20] J.D. Atkinson, B.J. Murray, D. O'Sullivan, Rate of homogeneous nucleation of ice in supercooled water, J. Phys. Chem. 120 (33) (2016) 6513–6520, https://doi.org/10.1021/acs.jpca.6b03843.
[21] G.C. Sosso, J. Chen, S.J. Cox, M. Fitzner, P. Pedevilla, A. Zen, A. Michaelides, Crystal nucleation in liquids: open questions and future challenges in molecular dynamics simulations, Chem. Rev. 116 (12) (2016) 7078–7116, https://doi.org/10.1021/acs.chemrev.5b00744.
[22] E. Sanz, C. Vega, J.R. Espinosa, R. Caballero-Bernal, J.L. Abascal, C. Valeriani, Homogeneous ice nucleation at moderate supercooling from molecular simulation, J. Am. Chem. Soc. 135 (40) (2013) 15008–15017, https://doi.org/10.1021/ja4028814.
[23] J. Yan, G. Patey, Heterogeneous ice nucleation induced by electric fields, J. Phys. Chem. Lett. 2 (20) (2011) 2555–2559, https://doi.org/10.1021/jz201113m.
[24] S. Karthika, T.K. Radhakrishnan, P. Kalaichelvi, A review of classical and nonclassical nucleation theories, Cryst. Growth Des. 16 (11) (2016) 6663–6681, https://doi.org/10.1021/acs.cgd.6b00794.
[25] L. Lupi, A. Hudait, V. Molinero, Heterogeneous nucleation of ice on carbon surfaces, J. Am. Chem. Soc. 136 (8) (2014) 3156–3164, https://doi.org/10.1021/ja411507a.
[26] R. Cabriolu, T. Li, Ice nucleation on carbon surface supports the classical theory for heterogeneous nucleation, Phys. Rev. E - Stat. Nonlinear Soft Matter Phys. 91 (5). doi:10.1103/PhysRevE.91.052402.
[27] Y. Bi, R. Cabriolu, T. Li, Heterogeneous ice nucleation controlled by the coupling of surface crystallinity and surface hydrophilicity, J. Phys. Chem. C 120 (3) (2016) 1507–1514, https://doi.org/10.1021/acs.jpcc.5b09740.
[28] B. Glatz, S. Sarupria, Heterogeneous ice nucleation: interplay of surface properties and their impact on water orientations, Langmuir 34 (3) (2018) 1190–1198, https://doi.org/10.1021/acs.langmuir.7b02859.
[29] F.K. Coradin, G.R. Possetti, R.C. Kamikawachi, M. Muller, J.L. Fabris, Etched fiber Bragg gratings sensors for water-ethanol mixtures: a comparative study, J. Microwaves Optoelectr. 9 (2) (2010) 131–143, https://doi.org/10.1590/S2179-10742010000200007.
[30] P. Aursand, M.A. Gjennestad, E. Aursand, M. Hammer, Ø. Wilhelmsen, The spinodal of single- and multi-component fluids and its role in the development of modern equations of state, Fluid Phase Equil. 436 (2017) 98–112, https://doi.org/10.1016/j.fluid.2016.12.018.
[31] K. Takaizumi, T. Wakabayashi, The freezing process in ethanol-water systems as revealed by differential scanning calorimetry, J. Solut. Chem. 26 (10). doi:10.1007/BF02768051.
[32] K. Koga, H. Yoshizumi, Diffential scanning calorimetry (DSC) studies on the freezing processes of water-ethanol mixtures and distilled spirits, J. Food Sci. 44 (5) (1979) 1386–1389, https://doi.org/10.1111/j.1365-2621.1979.tb06444.x.
[33] H.J. Borchardt, F. Daniels, The application of differential thermal analysis to the study of reaction kinetics, J. Am. Chem. Soc. 79 (1) (1957) 41–46, https://doi.org/10.1021/ja01558a009.
[34] R. Anderson, R. Adams, B. Duggins, Limitations of thermocouples in temperature measurements, in: 25th ISA Anaheim CA, 1979, pp. 1–33.
[35] J.M. Campbell, F.C. Meldrum, H.K. Christenson, Is ice nucleation from supercooled water insensitive to surface roughness? J. Phys. Chem. C 119 (2) (2015) 1164–1169, https://doi.org/10.1021/jp5113729.
[36] A. Dewaele, J.H. Eggert, P. Loubeyre, R. Le Toullec, Measurement of refractive index and equation of state in dense He, H2, H2O and Ne under high pressure in a diamond-anvil cell, Phys. Rev. B 67 (9) (2003), 094112, https://doi.org/10.1103/PhysRevB.67.094112.
[37] D. Lee, R. Haynes, D. Skeen, Properties of optical fibres at cryogenic temperatures, Mon. Not. Roy. Astron. Soc. 326 (2) (2001) 774–780, https://doi.org/10.1046/j.1365-8711.2001.04630.x.
[38] M. Boerkamp, D.W. Lamb, P.G. Lye, Investigating surface crystal growth using an intrinsic exposed core optical fibre sensor, Sensor. Actuator. B Chem. 157 (2) (2011) 581–585, https://doi.org/10.1016/j.snb.2011.05.026.
[39] P. Mani, A. Rallapalli, V.R. Machavaram, A. Sivaramakrishna, Monitoring phase changes in supercooled aqueous solutions using an optical fiber Fresnel reflection sensor, Optic Express 24 (5) (2016) 5395, https://doi.org/10.1364/OE.24.005395.
[40] W. Han, M. Rebow, D. Liu, G. Farrell, Y. Semenova, Q. Wu, Optical fiber Fresnel reflection sensor for direct detection of the solid–liquid phase change in n-octadecane, Meas. Sci. Technol. 29 (12) (2018), https://doi.org/10.1088/1361-6501/aaeabb, 125107.
[41] R. Kumar, W. Han, D. Liu, W.P. Ng, R. Binns, K. Busawon, Y.Q. Fu, Z. Ghassemlooy, C. Underwood, K. Mahkamov, J. Yuan, C. Yu, H. Shu, X.A. Li, T. Guo, G. Farrell, Y. Semenova, Q. Wu, Optical fibre sensors for monitoring phase transitions in phase changing materials, Smart Mater. Struct. 27 (10) (2018), https://doi.org/10.1088/1361-665X/aaddba, 105021.
[42] W. Han, M. Rebow, X. Lian, D. Liu, G. Farrell, Q. Wu, Y. Ma, Y. Semenova, SNS optical fiber sensor for direct detection of phase transitions in C18H38 n-alkane material, Exp. Therm. Fluid Sci. 109 (2019), 109854, https://doi.org/10.1016/j.expthermflusci.2019.109854. November 2018.
[43] A.D. Kersey, M.A. Davis, H.J. Patrick, M. LeBlanc, K.P. Koo, Fiber grating sensors, J. Lightwave Technol. 15 (8) (1997) 1442–1463, https://doi.org/10.1109/50.618377.
[44] R.C. Kamikawachi, I. Abe, A.S. Paterno, H.J. Kalinowski, M. Muller, J.L. Pinto, J.L. Fabris, Determination of thermo-optic coefficient in liquids with fiber Bragg grating refractometer, Optic Commun. 281 (4) (2008) 621–625, https://doi.org/10.1016/j.optcom.2007.10.023.
[45] Y. Saito, J.J. Wang, D.A. Smith, D.N. Batchelder, A simple chemical method for the preparation of silver surfaces for efficient SERS, Langmuir 18 (8) (2002) 2959–2961, https://doi.org/10.1021/la011554y.
[46] M.S. Wahl, Ø. Wilhelmsen, D.R. Hjelme, Addressing challenges in fabricating reflection-based fiber optic interferometers, Sensors 19 (18) (2019) 4030, https://doi.org/10.3390/s19184030.
[47] K. Takaizumi, A curious phenomenon in the freezing-thawing process of aqueous ethanol solution, J. Solut. Chem. 34 (5) (2005) 597–612, https://doi.org/10.1007/s10953-005-5595-6.
[48] S. Facq, F. Danède, B. Chazallon, Ice particle crystallization in the presence of ethanol: an in situ study by Raman and X-ray diffraction, J. Phys. Chem. 117 (23) (2013) 4916–4927, https://doi.org/10.1021/jp4015614.
[49] G.M. Kontogeorgis, E.C. Voutsas, I.V. Yakoumis, D.P. Tassios, An equation of state for associating fluids, Ind. Eng. Chem. Res. 35 (11) (1996) 4310–4318, https://doi.org/10.1021/ie9600203.
[50] A.J. Queimada, C. Miqueu, I.M. Marrucho, G.M. Kontogeorgis, J.A.P. Coutinho, Modeling vapor-liquid interfaces with the gradient theory in combination with the CPA equation of state, Fluid Phase Equil. 228 (2005) 479, https://doi.org/10.1016/j.fluid.2004.08.011.
[51] M. Oliveira, I. Marrucho, J. Coutinho, A. Queimada, Surface tension of chain molecules through a combination of the gradient theory with the CPA EoS, Fluid Phase Equil. 267 (1) (2008) 83–91, https://doi.org/10.1016/j.fluid.2008.02.020.
[52] M. Hongo, T. Hibino, Measurement of vapor-liquid-equilibria of binary and ternary-systems containing 1-propanol, water and calcium-chloride at 298.15 K, Kagaku Kogaku Ronbunshu 15 (4) (1989) 863–867, https://doi.org/10.1252/kakoronbunshu.15.863.
[53] J. Hu, C.A. Haynes, A.H. Wu, C.M. Cheung, M.M. Chen, E.G. Yee, T. Ichioka, K. Nishikawa, P. Westh, Y. Koga, Chemical potential and concentration fluctuation in some aqueous alkane-mono-ols at 25°C, Can. J. Chem. 81 (2) (2003) 141–149.
[54] A. Kotsarenko, N. Yarymazaev, V. Kalinichenko, Pressure isotherms of saturated vapor over the diethylene glycol water-methanol system from 251.95 K to 298.15 K, J. Appl. Chem. USSR 62 (8) (1989) 1750–1752.
[55] A. Shalmashi, F. Amani, Densities and excess molar volumes for binary solution of water + ethanol, + methanol and + propanol from (283.15 to 313.15) K, Lat. Am. Appl. Res. 44 (2) (2014) 163–166.
[56] A. Aasen, D. Reguera, Ø. Wilhelmsen, Curvature corrections remove the inconsistencies of binary classical nucleation theory, Phys. Rev. Lett. 124 (2020), 045701, https://doi.org/10.1103/PhysRevLett.124.045701.
[57] Ø. Wilhelmsen, D. Bedeaux, D. Reguera, Communication: tolman length and rigidity constants of water and their role in nucleation, J. Chem. Phys. 142 (17) (2015), https://doi.org/10.1063/1.4919689, 171103.

[58] R. Feistel, W. Wagner, A new equation of state for H2O ice Ih, J. Phys. Chem. Ref. Data 35 (2) (2006) 1021–1047, https://doi.org/10.1063/1.2183324.
[59] Ø. Wilhelmsen, A. Aasen, G. Skaugen, P. Aursand, A. Austegard, E. Aursand, M.A. Gjennestad, H. Lund, G. Linga, M. Hammer, Thermodynamic modeling with equations of state: present challenges with established methods, Ind. Eng. Chem. Res. 56 (13) (2017) 3503–3515, https://doi.org/10.1021/acs.iecr.7b00317.
[60] B. Zobrist, T. Koop, B.P. Luo, C. Marcolli, T. Peter, Heterogeneous ice nucleation rate coefficient of water droplets coated by a nonadecanol monolayer, J. Phys. Chem. C 111 (5) (2007) 2149–2155, https://doi.org/10.1021/jp066080w.
[61] P. Montero de Hijes, J.R. Espinosa, C. Vega, E. Sanz, Ice growth rate: temperature dependence and effect of heat dissipation, J. Chem. Phys. 151 (4) (2019), 044509, https://doi.org/10.1063/1.5103273.
[62] P. Montero de Hijes, J.R. Espinosa, E. Sanz, C. Vega, Interfacial free energy of a liquid-solid interface: its change with curvature, J. Chem. Phys. 151 (14) (2019), https://doi.org/10.1063/1.5121026, 144501.
[63] L. Ickes, A. Welti, C. Hoose, U. Lohmann, Classical nucleation theory of homogeneous freezing of water: thermodynamic and kinetic parameters, Phys. Chem. Chem. Phys. 17 (8) (2015) 5514–5537, https://doi.org/10.1039/c4cp04184d.
[64] T. van Westen, R.D. Groot, Predicting the kinetics of ice recrystallization in aqueous sugar solutions, Cryst. Growth Des. 18 (4) (2018) 2405–2416, https://doi.org/10.1021/acs.cgd.8b00038.
[65] J.R. Espinosa, C. Vega, E. Sanz, Ice–water interfacial free energy for the TIP4P, TIP4P/2005, TIP4P/Ice, and mW models as obtained from the mold integration technique, J. Phys. Chem. C 120 (15) (2016) 8068–8075, https://doi.org/10.1021/acs.jpcc.5b11221.
[66] M. Warkentin, J.P. Sethna, R.E. Thorne, Critical droplet theory explains the glass formability of aqueous solutions, Phys. Rev. Lett. 110 (1) (2013), 015703, https://doi.org/10.1103/PhysRevLett.110.015703.
[67] C.A. Jeffery, P.H. Austin, Homogeneous nucleation of supercooled water: results from a new equation of state, J. Geophys. Res.: Atmospheres 102 (D21) (1997) 25269–25279, https://doi.org/10.1029/97JD02243.
[68] R.S. Smith, B.D. Kay, The existence of supercooled liquid water at 150 K, Nature 398 (6730) (1999) 788, https://doi.org/10.1038/19725.
[69] J. Frenkel, Note on a relation between the speed of crystallization and viscosity, Phisik. Zeit. Sowjetunion 1 (1932) 498–510.
[70] S. Wu, Z. He, J. Zang, S. Jin, Z. Wang, J. Wang, Y. Yao, J. Wang, Heterogeneous ice nucleation correlates with bulk-like interfacial water, Sci. Adv. 5 (4) (2019), eaat9825, https://doi.org/10.1126/sciadv.aat9825.
[71] N.E. Dorsey, The freezing of supercooled water, Trans. Am. Phil. Soc. 38 (3) (1948) 247, https://doi.org/10.2307/1005602.
[72] J.A. Lange, Lange's Handbook of Chemistry, fifteenth ed., McGraw-Hill, Inc., New York, 1999.
[73] A. Chapoy, R. Anderson, H. Haghighi, T. Edwards, B. Tohidi, Can n-propanol form hydrate? Ind. Eng. Chem. Res. 47 (5) (2008) 1689–1694, https://doi.org/10.1021/ie071019e.
[74] B.Y. Okamoto, R.H. Wood, P.T. Thompson, Freezing points of aqueous alcohols. Free energy of interaction of the CHOH, CH2, CONH and C=C functional groups in dilute aqueous solutions, J. Chem. Soc., Faraday Trans. 1: Phys. Chem. Condens. Phases 74 (1978) 1990, https://doi.org/10.1039/f19787401990.
[75] H.R. Pruppacher, Interpretation of experimentally determined growth rates of ice crystals in supercooled water, J. Chem. Phys. 47 (5) (1967) 1807–1813, https://doi.org/10.1063/1.1712169.
[76] T. Buttersack, S. Bauerecker, Critical radius of supercooled water droplets: on the transition toward dendritic freezing, J. Phys. Chem. B 120 (3) (2016) 504–512, https://doi.org/10.1021/acs.jpcb.5b09913.
[77] S. Bauerecker, P. Ulbig, V. Buch, L. Vrbka, P. Jungwirth, Monitoring ice nucleation in pure and salty water via high-speed imaging and computer simulations, J. Phys. Chem. C 112 (20) (2008) 7631–7636, https://doi.org/10.1021/jp711507f.
[78] W.S. Price, H. Ide, Y. Arata, Solution dynamics in aqueous monohydric alcohol systems, J. Phys. Chem. 107 (24) (2003) 4784–4789, https://doi.org/10.1021/jp027257z.
[79] J.R. Espinosa, C. Navarro, E. Sanz, C. Valeriani, C. Vega, On the time required to freeze water, J. Chem. Phys. 145 (21) (2016), https://doi.org/10.1063/1.4965427, 211922.